Source parameters and moment tensor of the ML 4.6 earthquake of November 19, 2011, southwest Sharm El-Sheikh, Egypt

Gad-Elkareem Abdrabou Mohamed *, **Khaled Omar**

National Research Institute of Astronomy and Geophysics, Helwan, Egypt

Abstract   The southern part of the Gulf of Suez is one of the most seismically active areas in Egypt. On Saturday November 19, 2011 at 07:12:15 (GMT) an earthquake of ML 4.6 occurred in southwest Sharm El-Sheikh, Egypt. The quake has been felt at Sharm El-Sheikh city while no casualties were reported. The instrumental epicenter is located at 27.69°N and 34.06°E. Seismic moment is 1.47 E + 22 dyne cm, corresponding to a moment magnitude Mw 4.1. Following a Brune model, the source radius is 101.36 m with an average dislocation of 0.015 cm and a 0.06 MPa stress drop. The source mechanism from a fault plane solution shows a normal fault, the actual fault plane is strike 358, dip 34 and rake -60, the computer code ISOLA is used.

Twenty seven small and micro earthquakes (1.5 ⩽ ML ⩽ 4.2) were also recorded by the Egyptian National Seismological Network (ENSN) from the same region. We estimate the source parameters for these earthquakes using displacement spectra. The obtained source parameters include seismic moments of 2.77E + 16–1.47E + 22 dyne cm, stress drops of 0.0005–0.0617 MPa and relative displacement of 0.0001–0.0152 cm.

© 2014 Production and hosting by Elsevier B.V. on behalf of National Research Institute of Astronomy and Geophysics.

1. Introduction

An earthquake measuring ML 4.6 and Mw 4.1 jolted southwest Sharm El-Sheikh, Egypt on November 19, 2011. Some

Sharm El-Sheikh residents and its surroundings felt the quake and no casualties were reported. Twenty seven aftershocks (1.5 ⩽ ML ⩽ 4.2) followed the main event.

To a better understanding of the internal deformation of this area a detailed study of these small earthquakes (including source parameters estimations and moment tensor determinations) has also been performed. The extraction of the source parameters of these small earthquakes is very important because they are too small to be included in the Global-Centroid-Moment-Tensor (CMT) solutions. This paper represents the source parameters of 28 earthquakes and moment tensor of the November 19, 2011 earthquakes using high-quality digital seismograms of ENSN. Moment tensors

* Corresponding author. Tel.: + 20 225583887; fax: + 20 225548020.
  E-mail address: godah85@yahoo.com (G.-E.A. Mohamed).

(MTs) represent key information for seismotectonic studies. A powerful tool for the MT calculation is the waveform inversion.

The southern part of the Gulf of Suez is one of the most seismically active areas in Egypt. In general, the southern part of the Gulf of Suez has been described as an area of significant intermediate magnitude earthquake activity (Gergawi and El Khashab, 1968; Bosworth and Taviani, 1996). The distribution of historical and recent earthquakes in the Gulf of Suez showed that, there is a concentration of the activity along the southern end of the Gulf of Suez near the junction with the Northern Red Sea (Maamoun et al., 1984; Kulhanek et al., 1992). The higher rate of activity in the southern end of the Gulf of Suez is mainly related to the adjustments in motion at the triple junction between the African plate, Arabian plate and Sinai microplate (Ben-Menahem et al., 1976; Daggett et al., 1986). Distribution of seismicity from 1997 to September 2012 is shown in Fig. 1.

2. General geology and tectonics

The northern Red Sea is underlain by a sequence of Messinian salt, because in the Late Miocene the Red Sea was connected to the Mediterranean but detached from the Indian Ocean, and the Mediterranean desiccation affected the Red Sea (Phillips and Ross, 1970). At present, the northern Red Sea is built of a series of elongated rifts and salt diapirs commonly ascend along their boundary faults (Mart and Hall, 1984; Mart and Ross, 1987).

The Red Sea has two northward extensions, the Suez and the Levant rifts (Fig. 2). The Suez Rift trends northwestwards so that the western margin of the Red Sea extends to merge with the western boundary of the Suez Rift. The Suez Rift

was faulted in the Miocene, jointly with the northern Red Sea, as indicated by early Miocene dykes in southern Sinai (Bartov et al., 1980), and by thick marine sediments of Miocene age in the rift (Garfunkel and Bartov, 1977). The composite vertical displacement of the uplifted margins of the Suez Rift and its subsided center reaches several kilometers. The rate of tectonic activity reduced considerably since the latest Miocene (Garfunkel and Bartov, 1977; Steckler, 1985), concurrently with the opening of Elat (Aqaba) Rift. Elat Rift, the southernmost segment of the Levant Rift started its structural development in the late Miocene when the rift floor subsided in several basins, but most of its tectonic evolution occurred since the Pliocene, when the rift floor subsided fast in the axial basins, and its margins were extensively uplifted and eroded there (Horowitz, 1987; Mart, 1991). The structural characteristic of downthrown elongated rifted trough and uplifted and eroded margins that distinguish the Red Sea (Phillips and Ross, 1970), is also characteristic to both the Levant Rift system (Mart, 1991) and the Suez Rift (Moretti, 1987; Steckler, 1985).

The Gulf of Suez occupies the central portion of a rift with a length of about 350 km and a width ranging between 60 and 80 km (Patton et al., 1994; El-Khadragy et al., 1999). It extends from Latitude 27°15′ N to 30°00′ N and 32°00′ to 34°15′ E. It is characterized by the absence of sea floor spreading and any type of lateral symmetry (Hoseny, 1985). The Gulf of Suez formed in the latest Oligocene to Early Miocene as the northwestern extension of the Red Sea (Robson, 1971; Garfunkel and Bartov, 1977; Meshref, 1990). The Gulf of Suez and the Red Sea represent two rift systems created by extensional movement more or less perpendicular to their border faults (Ben-Avraham et al., 1979; Garfunkel et al., 1981). During the Middle Miocene, the opening of the Suez rift died out and the Red Sea rift propagated to the NNE direction, causing left-lateral strike-slip displacement of extensional component
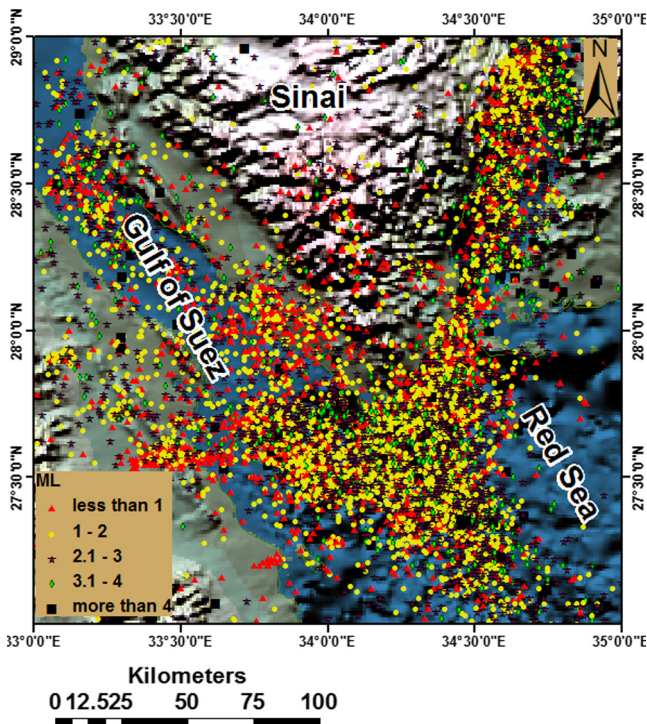

Fig. 1 Seismicity map from 1997 to September 2012 after Egyptian National Seismological Network (ENSN).
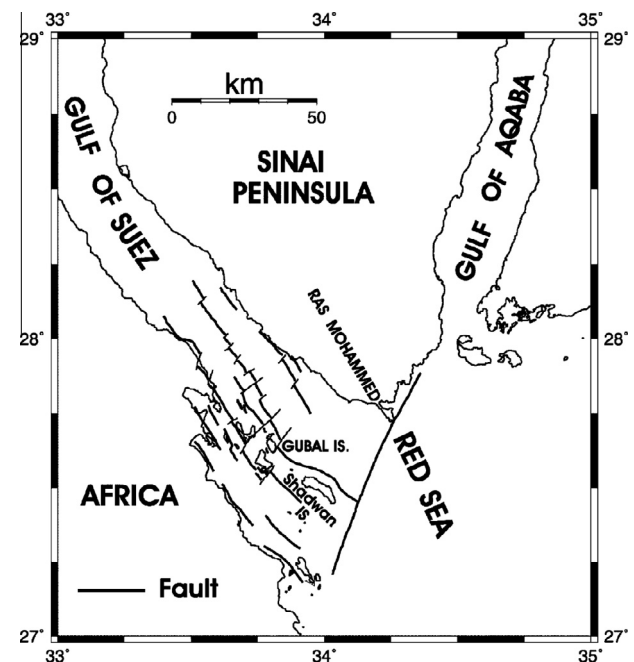

Fig. 2 Summary map of southern Gulf of Suez (after Bosworth, 1994).

on the Dead Sea Fault System (Quenell, 1958; Steckler and Ten Brink, 1986; Bosworth and McClay, 2001).

As in most extensional systems, the Gulf of Suez rift is controlled by normal faults and tilted blocks (Colleta et al., 1988). The fault pattern consists of two major sets: (1) the main clysmic fault trend (N 40°–30° W), that contains normal faults parallel to the rift axis and created during Neogene times in a pure extensional regime (Said, 1962; Meshref et al., 1976; Bartov et al., 1980; Jarrige et al., 1986; Colleta et al., 1988). (2) Transfer faults with NNE, WNW and ENE trends (Patton et al., 1994). The NNE and WNW faults trend oblique to the clysmic trend (Salman, 1982; El-Khadragy et al., 1999; Youssef et al., 2000). Faults belonging to these trends show predominant normal dip-slip component and very small strike-slip components (Moustafa, 1993, 2004). A summary map of the Gulf of Suez faults is shown in Fig. 2.

3. Moment tensor solutions

The computer code ISOLA is used, combining the computational speed of Fortran and the users' comfort of Matlab (Sokos and Zahradnik, 2008). It makes use of the inverse-problem formulation of Kikuchi and Kanamori (1991), based on six elementary MTs. Their Eq. (6) is used to quickly evaluate the correlation between observed and synthetic waveforms. Green's functions are calculated by the discrete-wavenumber method (Coutant, 1990; Bouchon, 2003). Besides Matlab graphics, GMT (Wessel and Smith, 1991) is used in all the stages of the procedure, in order to produce publication-quality figures of the retrieved moment tensors. The M_map software package is also used mainly for plotting maps within the Matlab environment.

ISOLA-GUI offers access to all the inversion procedures through modules that perform specific tasks, e.g. data import, filter, inversion, plotting, etc. Modules can run in parallel and most of them "remember" user's response or try to suggest suitable values of the parameters, in order to speed up the processing. Although most of the input parameters are self-explanatory, "tooltips" have been added for some of them. However these are not a substitute of the program's manual, which contains an extensive description of the method with examples. The user is urged to study the manual prior to the application of the inversion.

3.1. Data analysis

We calculate Moment tensor of the November 19, 2011 at 07:12:15 (GMT) earthquake of ML 4.6 by using ISOLA program by using six broad band stations (HRG, NADB, FRF, TAMR, SH2, NBNS). For the earthquake location, see Table 1 and Fig. 3. ISOLA's native format is quite simple (4 column ascii files, i.e., time, NS, EW, Z component) an option for format conversion from SAC and Guralp Compressed Format to ISOLA native format, is provided. The conversion is accomplished using Matlab codes (m-files) (Thorne, 2005). Besides the format conversion, a few options are provided for data quality assessment prior to moment tensor inversion, like various filters, perform instrument correction, integrate or shift

Table 1 Hypocentrals and source parameters calculated for events.

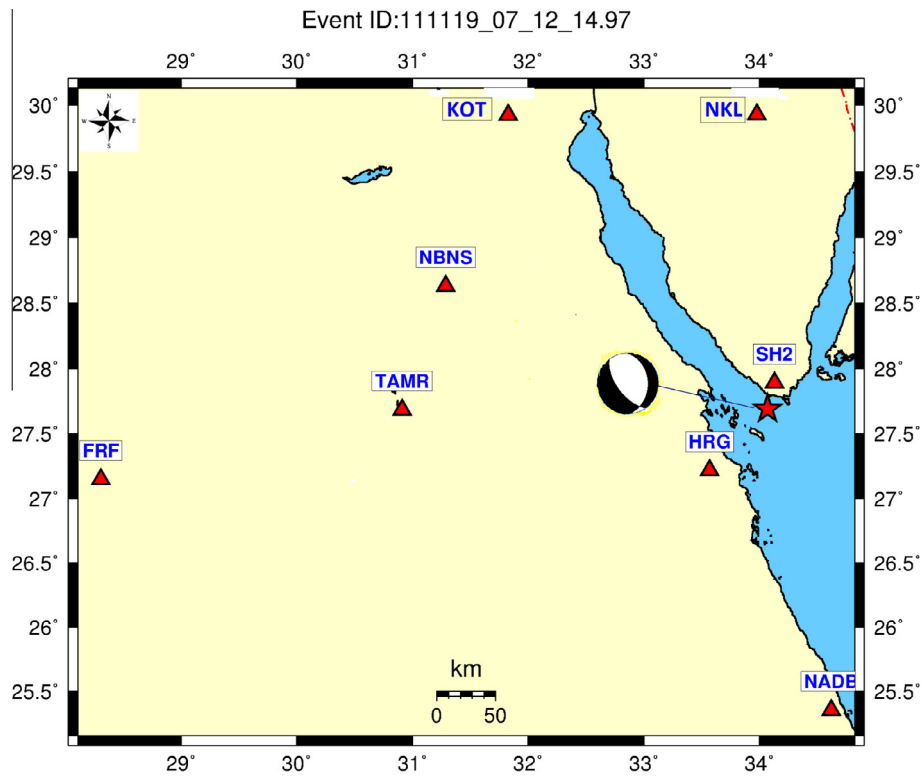| dd/mm/yy hh:mm	Lat. (N)	Lon. (E)	Depth (Km)	Mag. (ML)	Ω_0 (cm-s)	f_c	M_0 (dyne cm)	r (m)	$\Delta\sigma$ (MPa)
19/11/2011 07:12	27.69	34.06	14.98	4.59	1.79E−08	23.73	1.47E+22	101.36	0.0617
19/11/2011 19:55	27.71	33.99	10.11	2.22	1.56E−09	24.10	1.28E+20	99.8	0.0056
2011/11/20 05:16	27.66	34.24	15.88	4.19	1.11E−08	24.17	9.12E+21	99.48	0.0406
2011/11/20 17:40	27.61	34.22	20.76	3.20	7.35E−10	23.44	6.02E+20	102.58	0.0025
2011/11/20 17:44	27.60	34.21	17.01	2.84	7.61E−10	24.29	6.24E+19	98.989	0.0028
2011/11/21 15:31	27.58	34.40	9.93	1.61	1.37E−09	24.25	1.12E+18	99.173	0.005
2011/11/21 16:10	27.61	34.42	19.90	2.06	4.41E−10	23.06	3.62E+19	104.28	0.0014
2011/11/21 22:06	27.80	34.00	17.33	1.91	4.13E−10	24.94	3.39E+19	96.395	0.0017
2011/11/22 00:16	27.66	34.19	7.89	1.62	2.98E−10	24.48	2.44E+18	98.240	0.0011
2011/11/23 03:55	27.70	34.06	22.17	2.56	4.43E−10	24.27	3.63E+19	99.060	0.0016
2011/11/23 19:44	27.51	34.34	24.48	1.98	3.94E−10	23.88	3.23E+18	100.68	0.0014
2011/11/25 23:41	27.65	33.83	20.99	2.29	9.32E−10	24.23	7.64E+19	99.22	0.0034
2011/11/26 04:43	27.50	34.00	10.61	2.73	7.22E−10	24.23	5.92E+19	99.24	0.0027
2011/11/27 05:06	27.70	34.04	8.72	3.14	1.17E−09	23.44	9.57E+20	102.5	0.0039
2011/11/27 05:54	27.69	34.02	5.78	2.52	4.11E−10	22.99	4.65E+19	104.58	0.0013
2011/12/06 00:22	27.62	34.30	7.42	1.80	2.21E−10	24.63	1.81E+18	97.62	0.0008
2011/12/07 22:50	27.69	33.97	4.00	2.39	3.60E−10	23.55	8.54E+18	102.08	0.0012
2011/12/08 13:14	27.62	34.42	12.83	2.00	1.93E−09	23.32	1.58E+19	103.10	0.0063
2011/12/09 00:36	27.68	34.05	12.42	2.18	3.31E−10	24.29	2.71E+19	98.97	0.0012
2011/12/09 21:13	27.68	34.07	15.91	1.92	5.85E−10	23.13	4.80E+18	103.94	0.0019
2011/12/10 13:56	27.80	34.37	4.94	1.76	9.65E−10	23.24	7.91E+17	103.45	0.0031
2011/12/19 02:36	27.70	33.98	7.18	1.92	3.22E−10	23.48	2.64E+18	102.41	0.0011
2011/12/22 02:21	27.63	34.20	22.34	1.96	3.59E−10	24.33	2.95E+18	98.82	0.0013
2011/12/29 03:18	27.71	34.04	20.93	1.76	3.37E−10	23.79	2.77E+16	101.08	0.0012
2011/12/29 06:45	27.68	34.18	13.49	2.04	4.08E−10	24.29	3.34E+19	99.00	0.0015
2011/12/29 08:17	28.01	34.40	6.80	2.18	5.09E−10	24.15	4.17E+19	99.55	0.0019
2011/12/29 14:41	27.68	34.07	15.59	1.45	1.37E−10	23.79	1.12E+18	101.08	0.0005
2011/12/31 01:54	27.64	34.33	22.99	2.10	4.17E−10	24.35	3.42E+19	98.72	0.0015

Fig. 3 Broadband stations (triangles), epicenter location of the event (star) and fault-plane solution (beach ball).

the data, etc. These tasks are of major importance since in many cases the data contain various spurious signals, e.g. trends that can affect the inversion, while at the same time these are not easily recognizable in the time series data (Zahradnik and Plesinger, 2005). It is therefore recommended that these tests are applied prior to any inversion attempt. The data pre-processing part (instrument correction, alignment, integration, decimation, etc.) must be carried out carefully, since any error introduced at this stage can cause significant errors in the inversion step (Fig. 4).

Green's function calculation is performed using the frequency wavenumber method (Bouchon, 1981). The code is written in Fortran but the user controls its use through the ISOLA-GUI, using the greenpre tool. We have tried to limit the number of input parameters as much as possible, thus the user has to specify only the maximum frequency of Green's function computation. Then the code automatically generates Green's functions and the corresponding elementary seismogram files, while at the same time it stores everything in the proper folders. Various helpful features are included, like a special option for automatic calculation of station weights, based on the maximum amplitude of the displacement record, and a tool for plotting correlation and focal mechanism vs source position and its time shift (Fig. 5).

Besides the correlation, the double couple percentage of the solution (DC%) can also be plotted, since in many cases it can provide indication about problematic inversion results. The correlation plot is quite important. The application of constraints may be desirable depending on the resolution of the inversion parameters. For example, for the case of low resolu-

tion the constrained (fixed) focal mechanism may prevent "wild jumping" of subevents in space and time.

The last step is the plotting of the inversion results, in particular the moment tensor solution and the best fit between data and synthetics (Fig. 6). Again, a special tool was designed, named plotres, which uses Matlab and GMT graphic capabilities to prepare quality plots of the results. The variance reduction per tested source and the corresponding focal mechanism can be plotted together on a graph in order to inspect the inversion convergence through the whole computation. An option for comparing the computed focal mechanism solution with the available first motion polarities is also available. The correlation between observed and synthetic seismograms, as a function of depth, is shown in Fig. 7, illustrating stability of the focal mechanism and the best-fitting depth of 17 km.

In Fig. 8, the DC% is plotted against the correlation for each "point" of the studied spatio-temporal domain. The main variation of the DC% comes from the temporal shifts; the DC% can get practically any value from 0% to 100%. The black Cross represents all grid search, the blue square is the best space position, while the red Concrete is the best time position.

4. Source parameters from spectral modeling

The study of earthquake-source parameters and faulting processes of small earthquakes is important for clarifying the scaling of earthquake sizes and stress drops. Although kinematic earthquake-source models are not satisfactory in
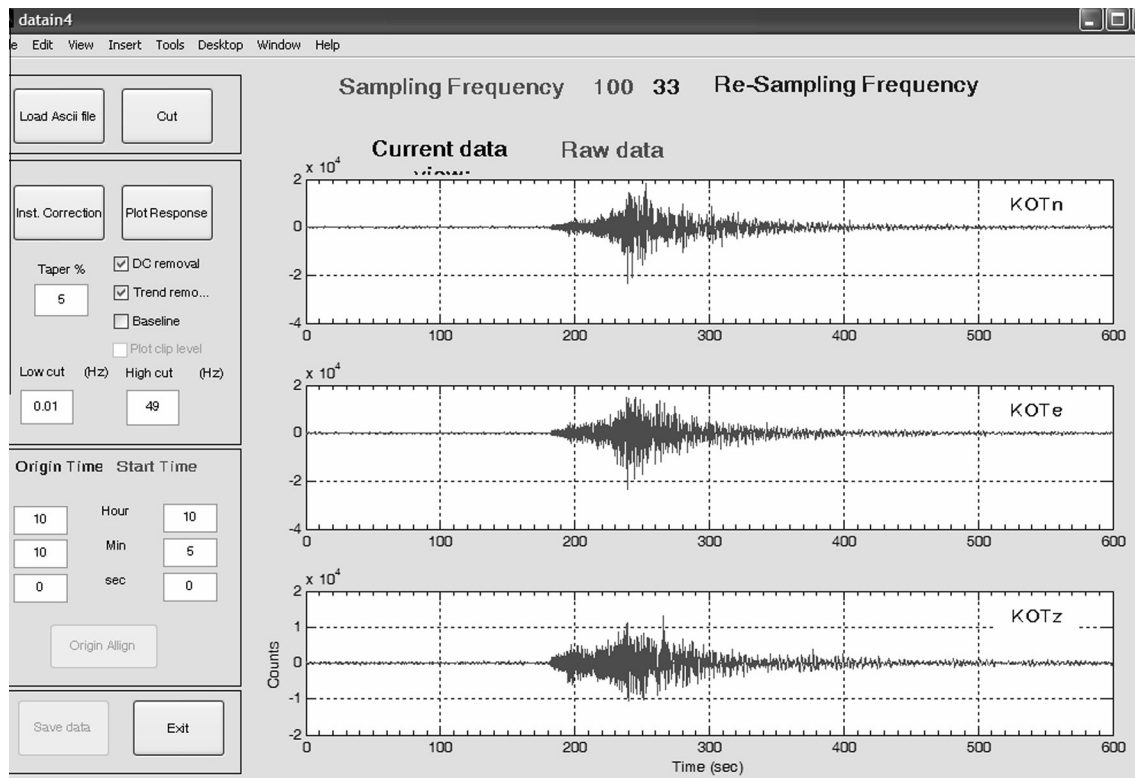
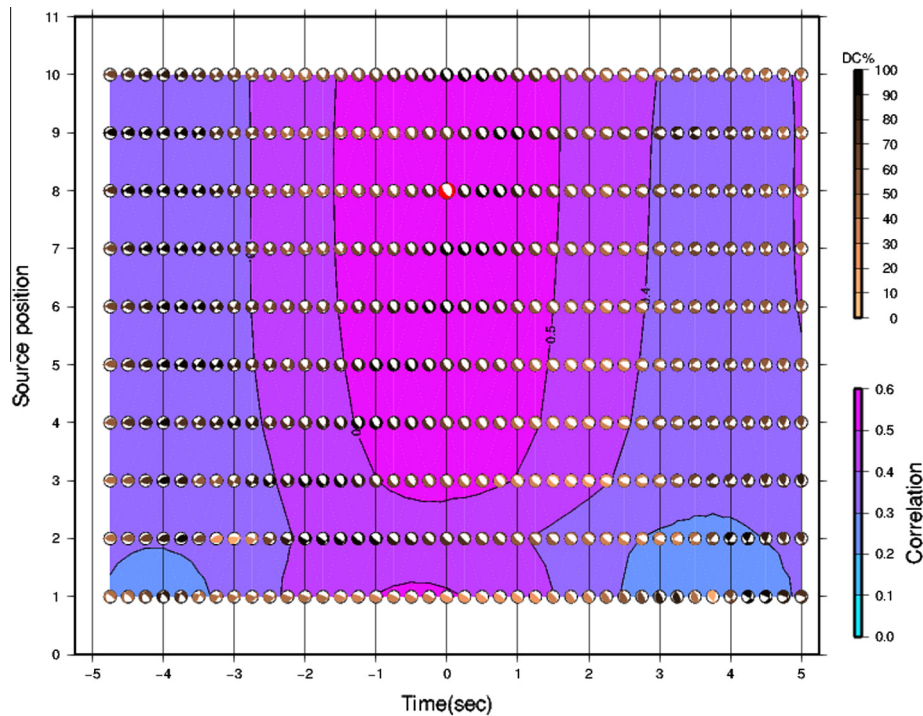Fig. 4   ISOLA-GUI tool for data pre-processing.

Fig. 5   Plot of correlation vs time shift, source position and focal mechanism for single source inversion. Largest correlation was obtained for source 2 (8 km depth) and 0.0 s time shift. Focal mechanism shading changes according to double couple percentage, while for diagram clarity, we only plot solutions having double couple percentage larger that 70%. Preferred solution is depicted by a larger beachball.
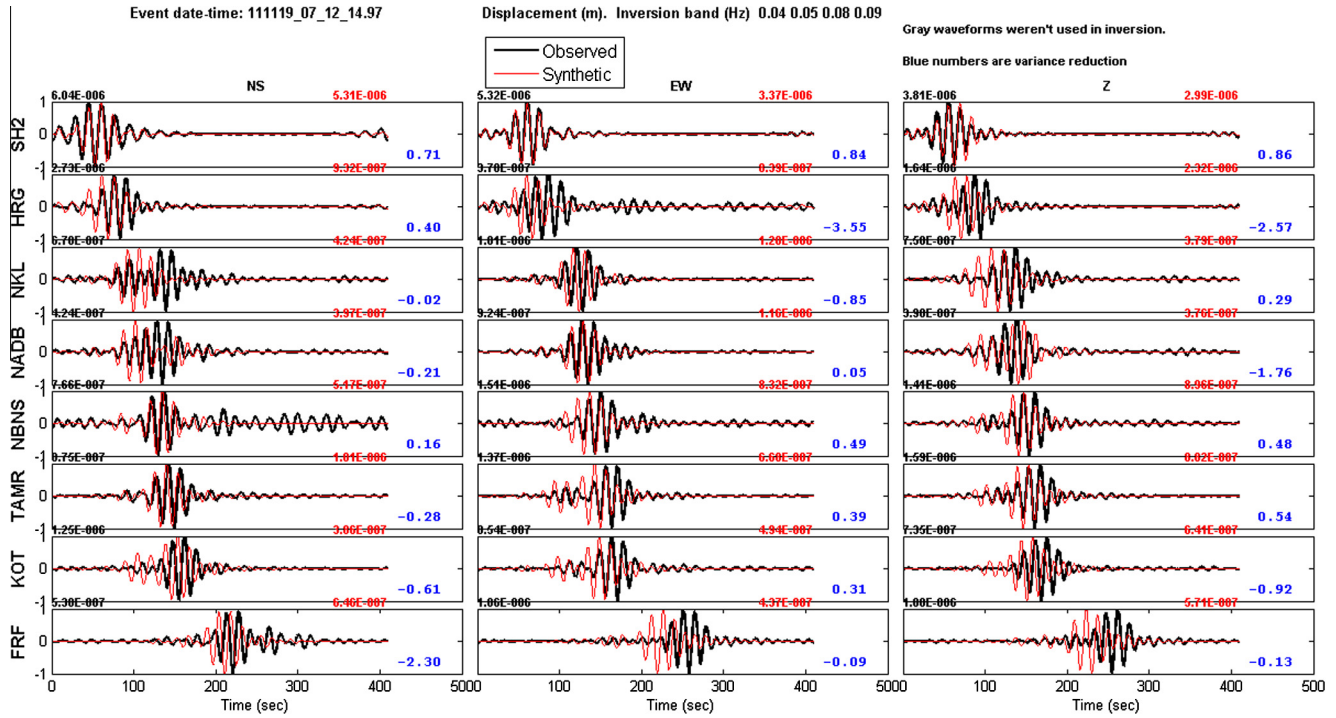
Fig. 6 Waveform comparison for single source inversion.
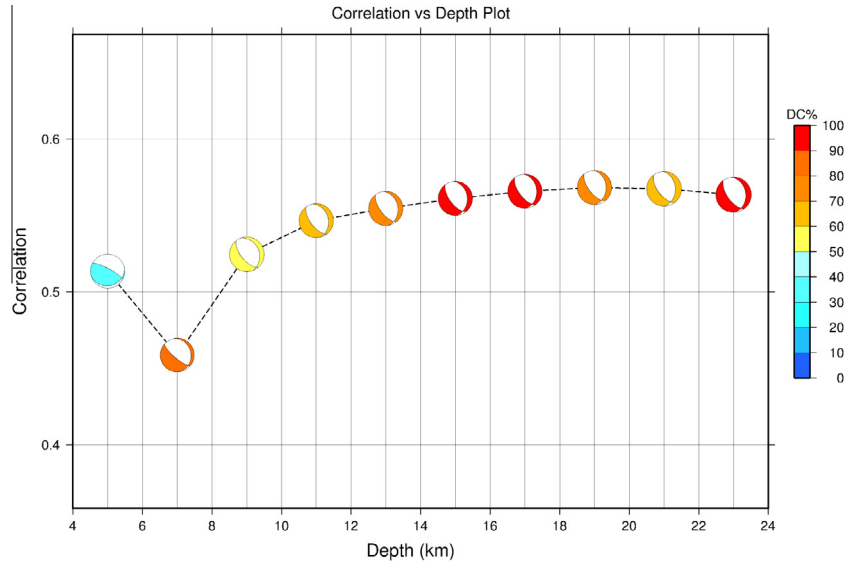

Fig. 7 The correlation between observed and synthetic waveforms and focal mechanism as a function of the trial source depth. Colors represent the DC%.

terms of rupture dynamics, they provide reliable results in terms of stress drop and coseismic slip distribution. Source parameter studies of microearthquakes are usually performed in the frequency domain and the spectra of the events are largely interpreted by using simple models (e.g. Aki, 1967; Brune, 1970; Madariaga, 1976; Boatwright, 1978, 1980).

To calculate the source parameters of the microearthquakes shown in Fig. 9, and Table 1 the records of vertical component to every station were corrected to zero baseline and instrument response. We selected 2 s P-wave signal windows that avoid contamination from other phases and maintain the resolution and stability of the spectra (Fig. 10).
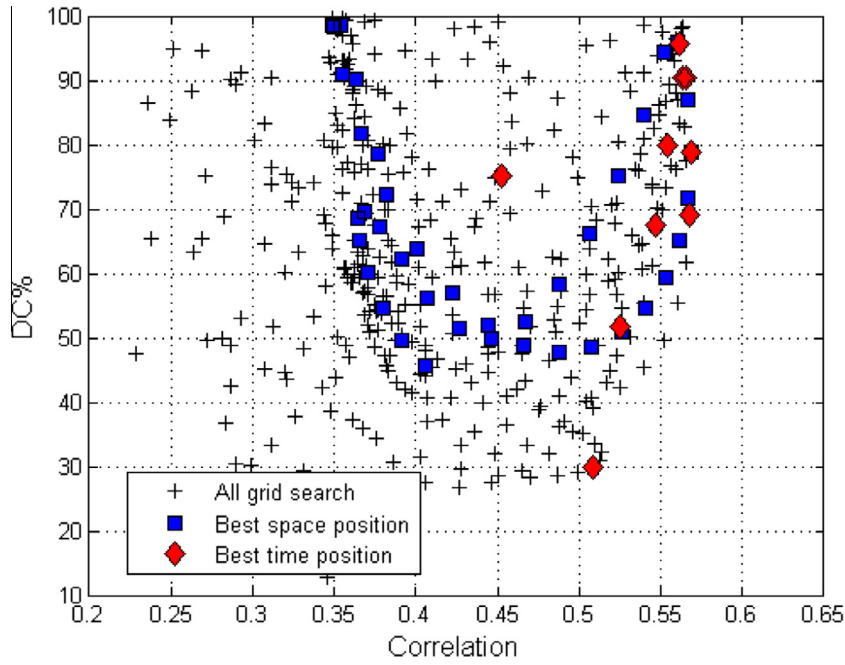
Fig. 8   The DC% versus correlation plot. Each *symbol* corresponds to a 'point' in the studied spatio-temporal grid.
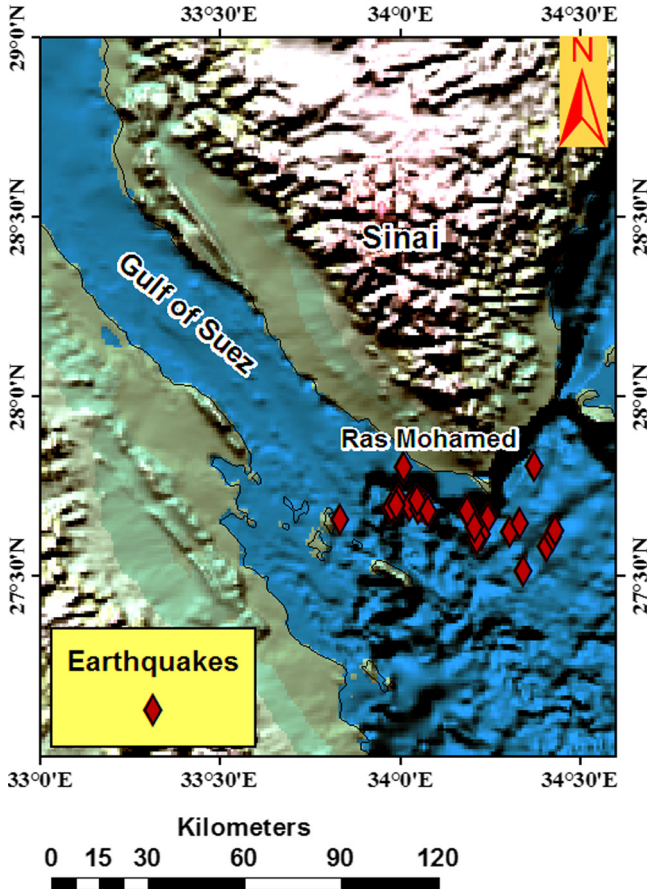

Fig. 9   Location of earthquakes which is used in this study.

The average spectrum was inverted using the simplified functional form of the source spectrum with a single corner frequency, described by the Boatwright (1978, 1980) equation:

$$S(f) = \Omega_0/[1 + (f/f_c)^{2\gamma}]^{1/2} \tag{1}$$

In Eq. (3), the spectral parameters Ω_o, fc, and γ represent the low-frequency amplitude level, the corner frequency, and the high-frequency spectral fall-off beyond the corner frequency, respectively. By assuming Brume's model ($\gamma = 2$).

Source parameters (seismic moment, stress drop, and source radius) were then calculated for a total of 28 events (Table 1). The seismic moment (M_0) was estimated by the following relationship (e.g. Brune, 1970):

$$M_0 = 4\pi\rho v^3 R\Omega_0/R_{(\theta,\varphi)} \tag{2}$$

where ρ is the density of the medium (2700 kg/m³), R is the hypocentral distance, v is the wave velocity, Ω_0 is the low frequency spectral amplitude and $R_{(\theta,\varphi)}$ is the radiation pattern coefficient. The estimated seismic moments (M_0) range between 1.12E + 16 and 1.47E + 18 dyne cm (Table 1).

The source radius (r) and the stress drop ($\Delta\sigma$) were calculated by the following equation Madariaga (1976):

$$r = 0.37v/f_c \tag{3}$$

where v is the wave velocity, f_c is the corner frequency of the wave.

$$\Delta\sigma = 7/16 \, (M_0/r^3) \tag{4}$$

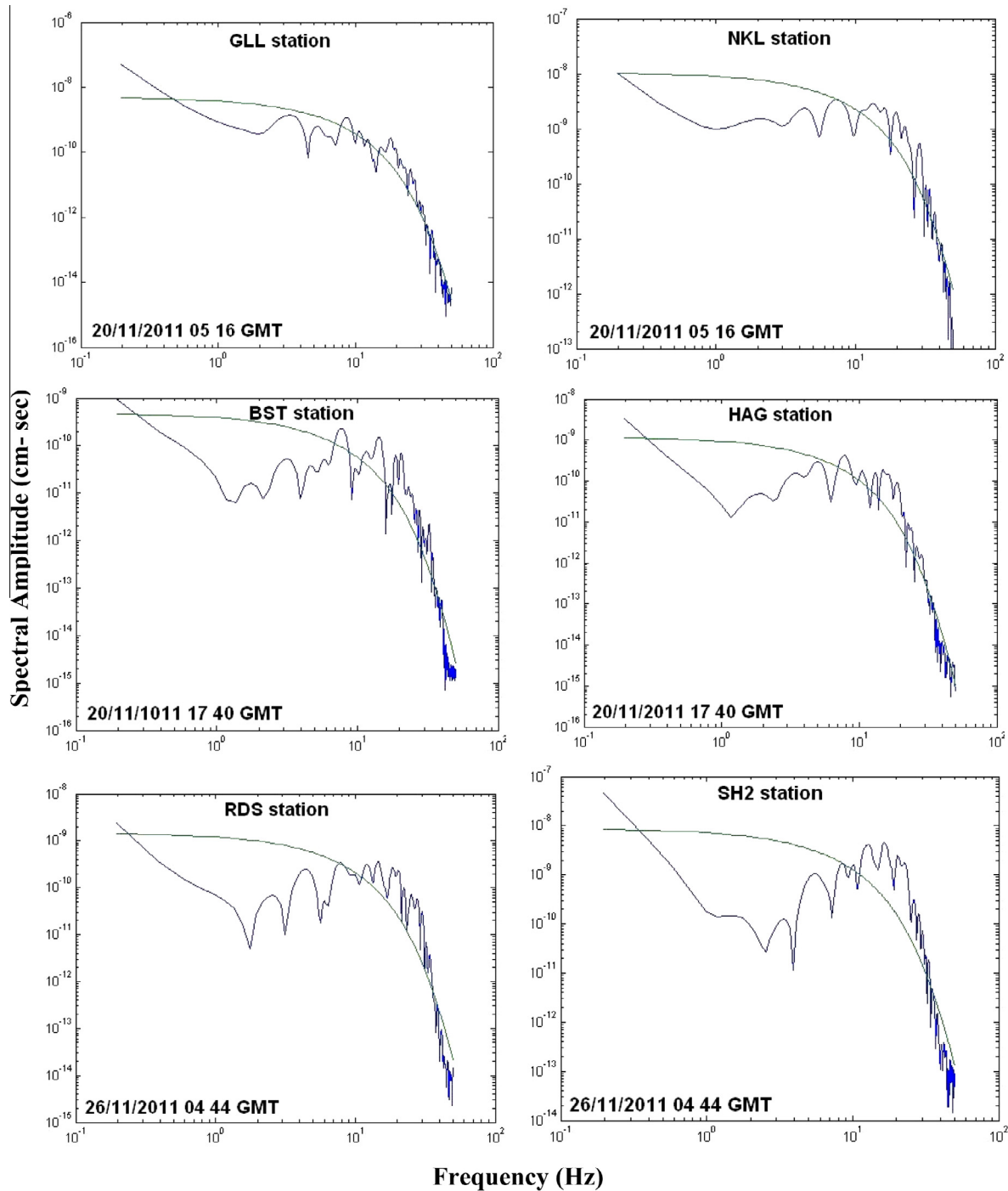where M_o is the seismic moment and r is the fault radius.

Fig. 10   Examples of earthquake spectra for some ENSN stations.

5. Discussion and conclusions

The source parameters of small earthquakes, including the felt event, at southeast Sharm El-Sheikh dislocation have been derived by using an inversion procedure for estimating the spectral parameters. Assuming a circular rupture area (Brune's model), the analyzed earthquakes give an average fault length ranging from 96.39 to 104.59 m and corresponding stress drops ranging from 0.005 to 0.0617 MPa. The obtained source

parameters indicate that the respective events could be considered as interplate earthquakes (Scholz et al., 1986).

The moment tensor analysis of local events is a standard procedure applied to broadband seismic networks from ENSN, in many cases even as an automatic procedure. In all such applications the inversion is performed for a single-point source. The programs ISOLA and ISOLA-GUI presented in this paper allow an easy application of the iterative deconvolution method of Kikuchi and Kanamori (1991), for local and

regional events, thus the method can be used for both single and multiple source geometry. The Matlab-based GUI facilitates easy data handling, while at the same time providing complete user control during all the processing steps and easy graphical display of the results, using both Matlab and GMT capabilities. The waveform inversion is done using the Fortran ISOLA code, in order to take advantage of language speed, while user interaction even during the inversion is within the Matlab environment. Various tools are available for the user to explore the data quality, adjust the computational parameters, correct the data, and display inversion results in a publication ready form. The modular design of the GUI allows the easy upgrade as well as the inclusion of user-created additional modules, using elementary skills in the Matlab programming language.

References

Aki, K., 1967. Scaling law of seismic spectrum. J. Geophys. Res. 72, 1217–1231.

Bartov, Y., Steinitz, G., Eyal, M., Eyal, Y., 1980. Sinistral movement along the Gulf of Aqaba; its age and relation to the opening of the Red Sea. Nature 285, 220–222.

Ben-Avraham, Z., Almagor, G., Garfunkel, Z., 1979. Sediments and structure of the Gulf of Elat(Aqaba), northern Red Sea. Sediment. Geol. 23, 239–267.

Ben-Menahem, A., Nur, A., Vered, M., 1976. Tectonics, seismicity and structure of the Afro-Eurasian Junction—the breaking of an incoherent plate. Phys. Earth Planet. Inter. 12, 1–50.

Boatwright, J., 1978. Detailed spectral analysis of two small New York state earthquakes. Bull. Seismol. Soc. Am. 69, 49–79.

Boatwright, J., 1980. A spectral theory for circular seismic sources: simple estimates of source dimension, dynamic stress drop and radiated energy. Bull. Seismol. Soc. Am. 70, 1–27.

Bosworth, W., 1994. A model for the three dimensional evolution of continental rift basins, northeast Africa. In: Schandelmeier, H., Stern, R.J. (Eds.), . In: Geology of Northeast Africa (Part 2), vol. 83. Geol. Rundsch., pp. 671–688.

Bosworth, W., McClay, K.R., 2001. Structural and stratigraphic evolution of the Gulf of Suez rift, Egypt: a synthesis. In: Ziegler, P.A., Cavazza, W., Robertson, A.H.F., Crasquin-Soleau, S. (Eds.), . In: Peri-Tethys Memoir 6: Peri-Tethyan Rift/Wrench Basins and Passive Margins, vol. 186. Memoires du Museum National d'Histoire Naturelle de Paris, pp. 567–606.

Bosworth, W., Taviani, M., 1996. Late Quaternary orientation of stress field and extension direction in the southern Gulf of Suez, Egypt: evidence from uplifted coral terraces, mesoscopic fault arrays and borehole breakouts. Tectonics 15 (4), 791–802.

Bouchon, M., 1981. A simple method to calculate Green's functions for elastic layered media. Bull. Seismol. Soc. Am. 71, 959–971.

Bouchon, M., 2003. A review of the discrete wavenumber method. Pure Appl. Geophys. 160, 445–465.

Brune, J.N., 1970. Tectonic stress and spectra of seismic shear waves from earthquakes. J. Geophys. Res. 75, 4997–5009.

Colleta, B., Lequellec, P., Letouzey, J., Moretti, I., 1988. Longitudinal evolution of the Suez Rift structure (Egypt). Tectonophysics 153, 221–233.

Coutant, O., 1990. Program of numerical simulation AXITRA. Laboratoire de Géophysique Interne et Tectonophysique Report. University of Joseph Fourier (in French).

Daggett, P., Morgan, P., Boulos, F.K., Hennin, S.F., el Sherif, A.A., El Sayed, A.A., Basta, N.Z., Melek, Y.S., 1986. Seismicity and active tectonics of the Egyptian Red Sea margin and the northern Red Sea margin and the northern Red Sea. Tectonophysics 125, 313–324.

El-Khadragy, A., El Gezeery, R.A., Ibrahim., S.A., Saada, S.A., 1999. Integrated geophysical interpretation of the surface geological conditions at the area north of Ras Gharib, Gulf of Suez, Egypt. In: Proceedings of the Seventeenth Annual Meeting, 17–18 March 1999. pp. 233–262.

Garfunkel, Z., Bartov, Y., 1977. The tectonics of the Suez Rift. Geol. Surv. Isr. Bull. 71, 1–44.

Garfunkel, Z., Zak, I., Freund, R., 1981. Active faulting in the Dead Sea Rift. Tectonophysics 80, 21–26.

Gergawi, A., El Khashab, H., 1968. Seismicity of the U.A.R.. Helwan Obs. Bull., 76.

Horowitz, A., 1987. Palynological evidence for the age and the rate of sedimentation along the Dead Sea Rift, and structural implications. Tectonophysics 141, 107–115.

Hoseny, H.M., 1985. Geophysical investigations in the Gulf of Suez consequences for the tectonic evolution of the northern Red Sea. Ph.D. Thesis. Keil University, Keil, Germany. p. 188.

Jarrige, J.J., Ott D' Estevou, P., Burollet, P.F., Icart, J.C., Montenat, C., Prat, P., Richert, J.P., Sehan, P., Thiriet, J.P., 1986. Inherited discontinuities and Neogene structure: the Gulf of Suez and the northwestern edge of the Red Sea. Philos. Trans. R. Soc. Lond. Ser. A 317, 129–139.

Kikuchi, M., Kanamori, H., 1991. Inversion of complex body waves—III. Bull. Seismol. Soc. Am. 81, 2335–2350.

Kulhanek, O., Korrat, I., El Sayed, A., 1992. Connection of the seismicity in the Red Sea and Egypt. In: Published Abstract in the 10th Annual Meeting of the Egyptian Geophysical Society, 1–3 March 1992.

Maamoun, M., Megahed, A., Allam, A., 1984. Seismicity of Egypt. HIAG Geophys. Bull. IV Ser. B 2, 109–160.

Madariaga, R., 1976. Dynamics of an expanding circular fault. Bull. Seismol. Soc. Am. 66, 639–666.

Mart, Y., 1991. The Dead Sea Rift: from continental rift to incipient ocean. Tectonophysics 197, 155–179.

Mart, Y., Hall, J.K., 1984. Structural trends in the northern Red Sea. J. Geophys. Res. 89, 11352–11364.

Mart, Y., Ross, D.A., 1987. Post-miocene rifting and diapirism in the northern Red Sea. Mar. Geol. 74, 173–180.

Meshref, W.M., 1990. Tectonic framework of Egypt. In: Said, R. (Ed.), The Geology of Egypt. A.A. Bakema, Rotterdam, pp. 113–155.

Meshref, W.M., Refai, E., Abdel-Baki, S., 1976. Structural interpretation of the Gulf of Suez and its oil potentialities. In: E.G.P.C. 5th Exploration Seminar, Cairo, Egypt.

Moretti, I., 1987. Modelisation de l'extension intracontinentale: example du golfe de Suez. Thesis. Université de Paris sud.

Moustafa, A.R., 1993. Structural setting and tectonic evolution of the east margin blocks of the Suez Rift. Tectonophysics 233, 381–399.

Moustafa, A.R., 2004. Geological Maps and Sections of Sinai Margin: AAPG Data Pages (CD Rom).

Patton, T.L., Moustafa, A.R., Nelson, R.A., Abdine, S.A., 1994. Tectonic evolution and structural setting of the Suez Rift. AAPG Mem. 59, 9–51.

Phillips, J.D., Ross, D.A., 1970. Continuous seismic reflexion profiles in the Red Sea. Philos. Trans. R. Soc. Lond. 267A, 143–152.

Quenell, A.M., 1958. The structural and geometric evolution of the Dead Sea Rift. Q. J. Geol. Soc. Lond. 114, 1–24.

Robson, D.A., 1971. The structure of the Gulf of Suez(Clysmic) rift, with special reference to the eastern side. J. Geol. Soc. 127, 274.

Said, R., 1962. Geology of Egypt. Elsevier, Amsterdam, p. 377.

Salman, A.B., 1982. Application of Landsat Imagery to Structural Interpretation and Exploration for Petroleum in the Gulf of Suez Environs, Egypt. The American University, Cairo Press, Cairo, A.R.E., pp. 1–27.

Scholz, C.H., Aviles, C.A., Wesnousky, S.G., 1986. Scaling differences between large interplate and intraplate earthquakes. Bull. Seismol. Soc. Am. 76 (1), 65–70.

Sokos, E., Zahradnik, J., 2008. ISOLA—a Fortran code and a Matlab GUI to perform multiple-point source inversion of seismic data. Comput. Geosci. 34, 967–977.

Steckler, M., 1985. Uplift and extension at the Gulf of Suez—indications of induced mantle convection. Nature 317, 135–139.

Steckler, M.S., Ten Brink, U.S., 1986. Lithospheric strength variations as a control on new plate boundaries: examples from the northern Red Sea Region. Earth Planet. Sci. Lett. 79, 120–132.

Thorne, M.S., 2005. Broadband waveform modelling of deep mantle structure. Ph.D. Dissertation. Arizona State University, United States. p. 283. Available from: <http://www.aeic.alaska.edu/> input/mthorne/pubs/index.htmlS.

Wessel, P., Smith, W.H.F., 1991. Free software helps map and display data, EOS. Trans. Am. Geophys. Union 72 (41), 445–446.

Youssef, M.I., El Sayed, A., Hammouda, H., Abu Shadi, F., 2000. Structural and tectonic patterns of the central area of the Gulf of Suez Rift, Egypt. In: International Conference on the Geology of the Arab World. Cairo University, February 2000. p. 274 (abstract).

Zahradnik, J., Plesinger, A., 2005. Long-period pulses in broadband records of near earthquakes. Bull. Seismol. Soc. Am. 95 (5), 1928–1939.